CARBON 77 (2014) 11–17

Available at www.sciencedirect.com

ScienceDirect

journal homepage: www.elsevier.com/locate/carbon

Multifrequency X,W-band ESR study on photo-induced ion radical formation in solid films of mono- and di-fullerenes embedded in conjugated polymers

A. Konkin [a,*], U. Ritter [a], P. Scharff [a], G. Mamin [b], A. Aganov [b], S. Orlinskii [b], V. Krinichnyi [c], D.A.M. Egbe [d], G. Ecke [a], H. Romanus [a]

[a] Center for Micro- and Nanotechnologies, Ilmenau University of Technology, Gustav-Kirchhoff-Str. 7, D-98693 Ilmenau, Germany
[b] Institute of Physics, Kazan Federal University, Kremlyovskaya St. 18, Kazan, Russia
[c] Department of Kinetics and Catalysis, Institute of Problems of Chemical Physics, Semenov Avenue 1, Chernogolovka, Russia
[d] Linz Institute for Organic Solar Cells, Altenberger Str. 69, A-4040 Linz, Austria

ARTICLE INFO

Article history:
Received 30 October 2013
Accepted 21 April 2014
Available online 4 May 2014

ABSTRACT

Anion–cation radical formation in solid films of M3EH-PPV blended with C_{60}-PCBM, C_{120}-O-PCBM and C_{60}-MDHE, C_{120}-O-MDHE under diode laser (532 nm) and Xe-lamp light excitation studied by means of X,W-band at temperatures 30–80 K is reported. Subsequent high frequency W-band ESR data demonstrate the reproducible, but variable effect of appreciable dispersion (*D*) contribution in the ESR spectral line for the di-fullerene anion radicals. It is suggested that the increase of the *D* part relative to the absorption (*A*) in the summarized ESR absorption line in blends with difullerenes is caused by the higher value of difullerene medium conductivity. The obtained data are quantitatively discussed by the $D/A \sim F(d/\delta)$ functional dependence in approach of plane film geometry, where *d* is the film thickness and δ is the skin-depth. The influence of ν-dependent δ at *D*/*A* value has been checked using X-band LESR.

1. Introduction

New effective electron acceptor composites for photovoltaics continue to be in the focus of goals for the application and understanding of the fundamental aspects of electron transfer in solid organic solar cells (OSCs). While mono-fullerenes and their various mono-adducts establish a good reputation as electron acceptors in mediums with conjugated polymers [1], wide popularity is however not the case for the fullerene dimmers and their adducts, mostly due to the lack of research on this subject. Regarding the possibility of di-fullerene use as electron acceptors in OSC blends, one feature should be considered beforehand, notably the possibility for registration of dianion/diradical formation under light excitation. In regard to monofullerenes, the reduction to $C_{60}^{(n-)}$ ($n = 2, 3, 4, 5$) can be obtained electrochemically and the corresponding oligo-radicals were certainly registered by ESR [2]. However, registration of the photo-induced *n*-anion in monofullerenes in

* Corresponding author.
E-mail address: alexander.konkin@tu-ilmenau.de (A. Konkin).
http://dx.doi.org/10.1016/j.carbon.2014.04.062
0008-6223/

experiments with conjugated polymer/fullerene blends has, to our knowledge, not been revealed. With respect to difullerenes the state of affairs is the same and the results of di-fullerene oligoanion formation has already been exhibited, for example in [3,4], where the reduction of $C_{120}O$ to $(C_{120}O)^{6-}$ was demonstrated electrochemically [3] and the reduction to $(C_{120}O)^{2-\cdot}$, $(C_{120}O)^{4-\cdot}$ and $(C_{120}OS)^{3-\cdot}$ was registered by ESR in [3] and [4], respectively. Our preliminary study of di-anion radical formation in C_{120}-O-PCBM:M3EH-PPV blends by X,K-band LESR [5], however, did not indicate triplet spin state features in ESR spectra under light excitation and supposes formation of the C_{120}-O-PCBM monoradical, which is supported by the W-band experiments introduced below. Nevertheless, the evident dispersion contribution in LESR spectra of di-fullerene/polymer films registered by the W-band LESR technique indirectly indicates a higher photoconductivity of difullerene medium in comparison with monofullerenes. This dispersion contribution should be studied by other methods, especially due to the recently reported results regarding two-dimensional organic metal based on fullerene [6], where the appreciable dispersion contribution is registered by ESR as well. Therefore, ESR photoconductivity detection in difullerene domains/nanoparticles is the dominating topic of this communication.

2. Experimental

The PCBM-$C_{120}O$ PCBM-C_{60}, MDHE-$C_{120}O$, and MDHE-C_{60} fullerenes and M3EH-PPV copolymers have been synthesized by the methods described in [7–9], respectively, and their chemical structures are shown in Fig. 1. Blends M3EH-PPV/(PCBM-$C_{120}O$, PCBM-C_{60}, MDHE-$C_{120}O$, and MDHE-C_{60}) were combined with a weight ratio of 1:1 w.r. and diluted in chlorobenzene under ultrasonic condition during 4 h. Composite films with a thickness of $d = 8 \pm 2$ μm were prepared via drop casting using a polyester foil substrate in X-band (9.5 GHz) and quartz capillary ($R = 0.2$ mm) in W-band (94 GHz) LESR experiments. The samples were dried under ambient conditions at room temperature. The electron spin echo (ESE) detected W-band (94 GHz) LESR spectra were recorded using a Bruker BioSpin spectrometer ELEXYS E680 and CW X-band (9.4 GHz) ESR spectra were recorded with an ELEXYS E500 under illumination provided by an optical fiber from a diode-laser (532 nm) at W-band and a Xe-lamp at X-band using an optical transmission resonator, ER 4104OR (Bruker BioSpin).

3. Results and discussion

All of the above mentioned M3EH-PPV/(mono and difullerene) blends (from here on in the text fullerene dimmers and their adducts will be only called difullerene) exhibit the effective charge separation (CS) process due to electron transfer from polymer to fullerenes and have been reliably registered by both X- and W-band LESR. Two well resolved anion/cation radical lines attributed to the positive polaron of M3EH-PPV (in figures denominated as P^+) and fullerene/difullerene anion radicals (R_{FA}) appeared under light illumination and their W-band LESR spectra recorded in the temperature range 20–80 K are shown in Fig. 2a and b. In addition to pure spectroscopic characterization, the main issue of consideration is devoted to detection of variable but consistently reproducible appreciable dispersion contribution in anion radical spectra of samples, including difullerenes in comparison to monofullerene derivatives. The comparison of mono- and difullerenes (PCBM and C_{120}-O-PCBM) with W-band LESR spectra recorded at the same temperature ($T = 50$ K in Fig. 2) has been the starting point of this study. The difullerene R_{FA} W-band LESR spectral line exhibits a form unusual for monofullerene anion radicals (like the R_{FA} line of PCBM/M3EH-PPV spectrum in Fig. 2a). It should be mentioned that the fullerene R_{FA} first derivative of the ESR absorption line looks like the Dysonian line shape, which normally indicates the dispersion contribution due to the conductivity of paramagnetic medium. However, in the case of fullerene anion radicals, the specific spectroscopic and spin dynamic parameters, notably $g_x \approx g_y > g_z$ and linewidth $\Delta_x \approx \Delta_y \ll \Delta_z$, are responsible for the R_{AF} line shape in the systems with randomly orientated paramagnetic centra relative to the direction of external magnetic field H (powder/glass spectrum). Therefore, the obvious ESR difullerene R_{AF} line shape transformation i.e. the deviation from the R_{FA} spectra often observed in the monofullerene can be described assuming dispersion contribution but with the opposite dispersion curve phase (negative sign). The above dispersion is observed experimentally in conductive 2D electron gas systems, for example in solid state semiconductors [10,11], and additionally a similar line shape is detected for the fullerene anion radicals in conductive metal doped fullerene

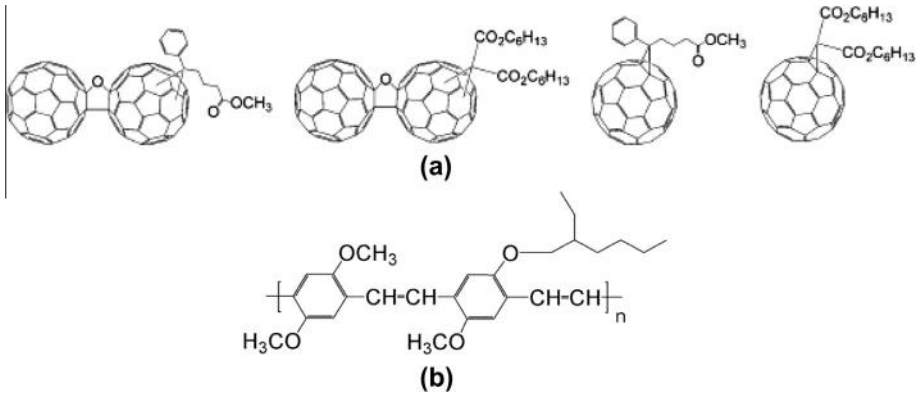

Fig. 1 – Composite structures: (a) from left to right are C_{120}-O-PCBM, C_{120}-O-MDHE, PCBM, C_{60}-MDHE (b) M3EH-PPV copolymer.

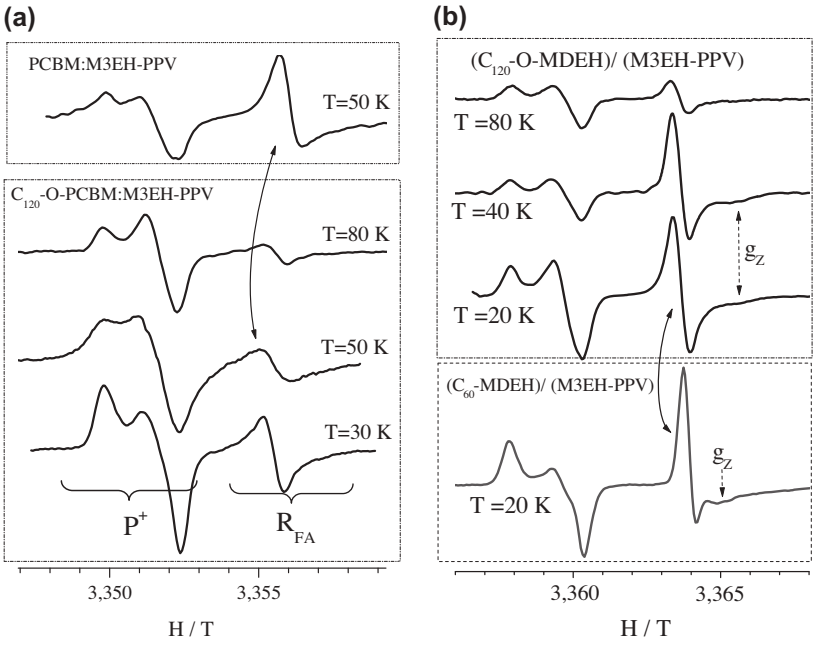

Fig. 2 – W-band experimental spectra of studied blends recorded over a temperature interval of 20–80 K: (a) PCBM:M3EH-PPV (T = 50 K), C_{120}-O-PCBM/M3EH-PPV (T = 30, 50, 80 K) (b), C_{60}-MDEH/M3EH-PPV (T = 20 K), C_{120}-O-MDHE/M3EH-PPV (T = 20, 50, 80 K).

composites [12]. The simulation of experimental spectra has been performed using the field derivative of the linear combination of both A and D normalized Lorentz shape functions:

$$Y'(L,\Delta,H_0) \propto -\frac{L(\Delta^2-(H-H_0)^2)+2\Delta(H-H_0)}{[\Delta^2+(H-H_0)^2]^2}, \quad (1)$$

where Δ – is the ESR line width, H_0 – is the resonance magnetic field, $L = P/Q$ is the parameter responsible for the relative dispersion contribution to the ESR line shape and P, Q are the functions of the sample adduced specimen $2d/\delta$, where $2d$ is the thickness of the plate (film) or cylinder radius and δ is the skin-depth ($L = 0$ gives the absorption contribution only). Although the X- and W-band experiments were carried out in resonators with different microwave eigenmode symmetry (rectangular and cylindrical respectively), it seems the samples thickness $d \ll r$ (cylinder capillary radius) and the comparison of two-frequency ESR results is a reasonable approach of flat film geometry, where

$$P = \frac{1}{p^2+q^2}\cdot\frac{q\cdot\sin h(p)-p\cdot\sin(q)}{\cos h(p)+\cos(q)}+\frac{\sin(q)\cdot\sin h(p)}{(\cos h(p)+\cos(q))^2}$$
$$Q = \frac{1}{p^2+q^2}\cdot\frac{p\cdot\sin h(p)+q\cdot\sin(q)}{\cos h(p)+\cos(q)}+\frac{\cos(q)\cdot\cos h(p)+1}{(\cos h(p)+\cos(q))^2}, \quad (2)$$

$p = (2d/\delta)\quad[(1+t^2)^{0.5}-t]^{0.5}$, $q = (2d/\delta)\quad[(1+t^2)^{0.5}+t]^{0.5}$, $\delta = (\pi\nu\mu_o\mu_r\sigma)^{-0.5}$, $t = \varepsilon\nu/2\sigma$, $\varepsilon = \varepsilon_o\varepsilon_r$ – permittivity (ε_R, μ_r and ε_o, μ_o are the relative and in vacuum permittivity and permeability, respectively), σ-conductivity, ν-oscillating magnetic field linear frequency [13]. It should be pointed out that the expressions of (2) are similar to the ones developed in [14] for the plane film configuration, but are expanded here to the more general case of samples with arbitrary dimensions and conductivities. W-band ESR spectral line simulation for the different L values has been carried out using expression (1)

$$Y \propto, \int_\alpha\int_\beta Y'[L,\Delta(\alpha,\beta),H_0(\alpha,\beta)]\sin(\alpha)d\alpha d\beta, \quad (3)$$

for the randomly orientated triaxial (X, Y, Z in inset 1 in Fig. 3) paramagnetic centre, (powder/glass spectrum) where $H_0 = \nu\gamma/g(\alpha,\beta)$, γ-electron magnetogyric ratio, effective g-factor $g(\alpha,\beta) = [(g_x\sin(\alpha)\sin(\beta))^2+(g_y\sin(\alpha)\cos(\beta))^2+(g_z\cos(\alpha))^2]^{1/2}$ and anisotropic line width $\Delta(\alpha,\beta) = [(\Delta_x\sin(\alpha)\sin(\beta))^2+(\Delta_y\sin(\alpha)\cos(\beta))^2+(\Delta_z\cos(\alpha))^2]^{1/2}$, where α, β are assigned to angles shown inside the X, Y, Z orthogonal coordinate system in inset 1 of Fig. 3.

The simulation results are shown in Fig. 3 and the essential changing of the asymmetry ratio between the positive/negative amplitude A/B (A and B are shown in Fig. 3) with dispersion contribution increase was positively registered (note that the A/B ratio is often used for the qualitative conductive properties characterization in comparative ESR spectra handling). The g-factors and line width values used in the simulations are introduced in captions of Fig. 3 and are similar to experimental ones. It should be emphasized that in this case the A/B ratio for R_{FA} depends on two features: (a) the contribution of the high field g_z spectral component (note that $\Delta_z \gg \Delta_x \approx \Delta_y$ at least 4 times larger and practically invisible in the spectrum taking into account that the amplitude $\propto 1/\Delta^2$), (b) the negative sign (opposite phase) of dispersion. The other experimental results are introduced in Figs. 2–5. The spectra of both difullerene derivatives blended with M3EH-PPV and recorded in the temperature range 20–80 K are shown in Fig. 2a and b. The spectra exhibit a weak temperature A/B deviation for each group but there is evidence difference in the A/B ratio between the blends ($A/B \approx 0.8$ for C_{120}-O-PCBM and $A/B \approx 1.2$ for C_{120}-O-MDHE, attributed to the different dispersion contribution, notably, $L \approx 1$ and $L \approx 0.35$, respectively). The above L determination can be carried out easily using the results introduced in Fig. 3 and its inset 2.

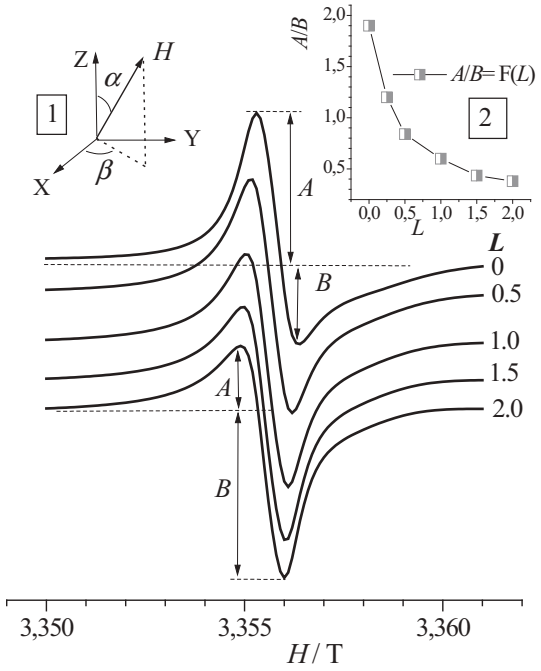

Fig. 3 – W-band spectra, simulated by (3) for different *L* values with $g_x = 2.0004$, $g_y = 2.00002$, $g_z = 1.9987$, $\Delta_x = 0.5$ mT, $\Delta_y = 0.5$ mT, $\Delta_z = 1.5$ mT). Inset 1 displays α,β angles as described in the text, assigned to a local coordinate system of a paramagnetic centre. Inset 2 shows the *A*/*B* ratio dependence as a function of *L*.

The examples of *L* values for R_{FA} in the monofullerene/M3EH-PPV spectra in Fig. 2a (PCBM, $T = 50$ K) , Fig. 2b (C_{60}-MDHE, $T = 20$ K) and Fig. 4b (C60-MDHE, $T = 80$ K) exhibit $A/B > 2$, therefore $L \approx 0$, which indicates the absence of dispersion contribution due to the results displayed in Fig. 3 and its inset. The examples of the direct P^+, R_{FA} X- and W-band spectra simulation by (3) are displayed in Figs. 4 and 5 and the results are gathered in Table 1. Taking into account the appreciable *L* dependence (see below Fig. 6) from the sample adduced specimen $2d/\delta$ (here ν-dependence should be in focus), the X-band spectra simulations for difullerene composites are important and performed as well. Assuming the same conductivity values for each blend it was suggested that the different ν, i.e. $\nu_X \sim 9.5$ GHz and $\nu_W \sim 94$ GHz for X-band and W-band, respectively are responsible for the different *L* values obtained from LESR spectra data handling (Table 1 and Fig. 6).

Note that due to the objective reason X-band spectra for C_{120}-O-MDHE and C_{60}-MDHE were recorded from blends with the P3HT polymer, however this cannot influence their R_{FA} spectra. Based on the above values of *L* obtained for differents ν, the consideration of the $L = F(X)$ function, where $X = 2d/\delta = 4\pi d(\nu\sigma)^{0.5}$, gives rise to estimate the photo-conductivity of the di-fullerene medium in both blends. In Fig. 6 the *L* dependence for both di-fullerene derivatives are shown. Taking into account the $L = P/Q$ dependence from parameter *t* (see denominations for *P* and *Q* in (2)), one can estimate preliminary the range of *t* values based at least on the monofullerene conductivity. For the estimation of *t*, a resistivity of about 0.6 mΩ cm for the K_3C_{60} film [15] has been taken which gives $t \approx 10^{-4}$. An increase of *t* up to 5×10^2 times does not have an influence in the *L* interval involved in our experimental values between 0 and 1 (area S restricted by the rectangle in Fig. 6). Therefore, in further discussion the *L* curve constructed for $t = 0$ has been used.

Five points A, B, C, D, E in Fig. 6b are included in consideration of experimental results: A, B, C relate to R_{FA} in the C_{120}-O-PCBM/M3EH-PPV blend, where $L_A = 1$, $L_B = 0.3$ are experimental values obtained in the W- and X-bands, respectively, which gives $X_A = 1.62$, $X_B = 0.92$. The ratio $X_A/X_B = 1.8$ does not coincide with the expected $(\nu_{Wb}/\nu_{Xb})^{0.5} \approx 3$ given from the calculated point C ($X_C = 0.54$ and $L_C = 0.1$), included in Fig. 6b for comparison. The above deviation has been attributed to the higher (above the average by 20%) film thickness in X-band experiments with the C_{120}-O-PCBM/M3EH-PPV blend. Variation of film thickness can certainly influence the *L* value. For example, a $2d$ size deviation of about 50% changes *L* by approximately 100%, which can be easily estimated from the *L* curve in Fig. 6. However, we cannot attribute the above difference only to the film thickness due to the possibility of different sizes of difullerene domains/nanoparticles (possibly $<2d$) formed inside films that cannot be checked by ESR as a result of average *L* detection. With respect to C_{120}-O-MDHE/M3EH-PPV blend results (points D and E in Fig. 6b), an analogous film thickness deviation has been registered, however the average is 10% and this cannot cause an appreciable influence at the position of X_E, at least in the interval $X = 0.3 \pm 0.05$. Therefore, $X_E = 0.3$ $(X_E = X_D/(\nu_{Wb}/\nu_{Xb})^{0.5} \approx X_D/3 = 1/3 = 0.3)$ as well as $X_D = 1$ correlate quite sufficiently with experimental values of $L_D = 0.35$ and $L_E = 0.035$, displayed in Fig. 6b. Taking into account that both di-fullerene R_{FA} ν-dependent *L* values coincide acceptably with the simulated $L = F(X)$ curve, the above result makes the estimation of skin depth δ of di-fullerene domain media possible. For the calculation the choice of point A in Fig. 6 ($X_A \approx 1.56$) i.e. W-band result for the C_{120}-O-PCBM anion radical appears reasonable. Therefore, considering that $\mu_r \approx 1$ for paramagnetic and assuming that the film thickness deviation is $2d \approx 16$ μm, for the ESR frequency around 95 GHz the skin depth δ is about 10 μm. It should be emphasized that here the above conductivity estimation by ESR is valid only for difullerene nanoparticles, not for their blend with the polymer. Unfortunately to check this result using a four contact method is a difficult task due to the presence of low conductivity of the thin polymer films/layers in the interface area between the difullerene domain/nanoparticles as well as between the film surface and electrodes. The above polymer covering of difullerene nanoparticles is supported by the Auger results introduced later in the text.

With regard to C_{120}-O-MDHE, W-band results give $X_D = 1$ and assuming approximately the same film thickness one can attain a σ reduction of about 3 times in comparison with C_{120}-O-PCBM. However, as was already emphasized in the abstract, the di-fullerenes R_{FA} spectra exhibit reproducible, but variable effects of significant dispersion contribution in the LESR spectral line. For example, for the three studied C_{120}-O-MDHE/M3EH-PPV blends the *L* values spanned an interval of 0.35–0.5, indicating a deviation of *X* as well and therefore the above conductivity comparison with C_{120}-O-PCBM/M3EH-PPV cannot be considered as definitely cor-

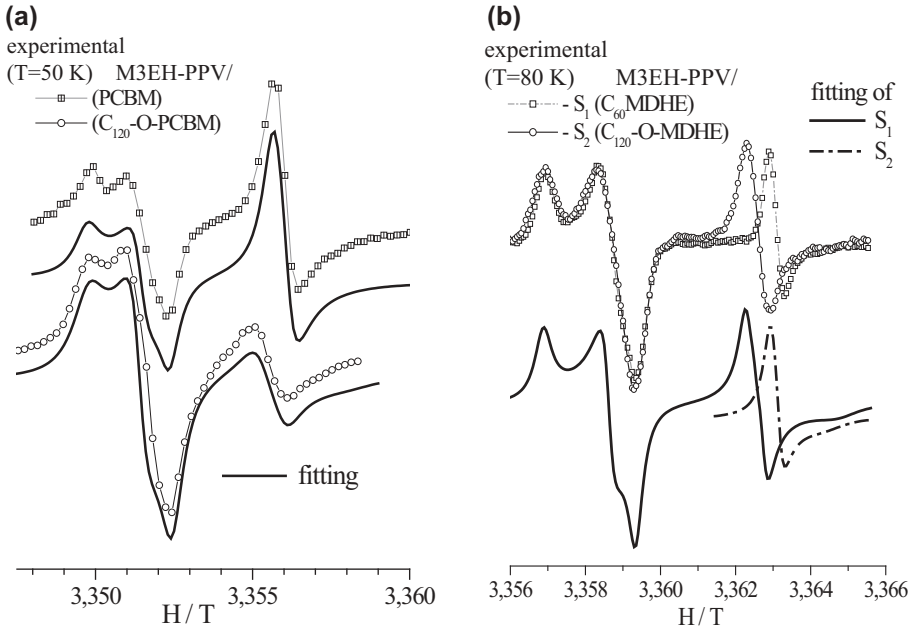

Fig. 4 – Experimental and fitted W-band spectra of PCBM/M3EH-PPV, C_{120}-O-PCBM/M3EH-PPV, C_{60}-MDHE/M3EH-PPV and C_{120}-O-MDHE/M3EH-PPV (spectra denominations are inside the figures).

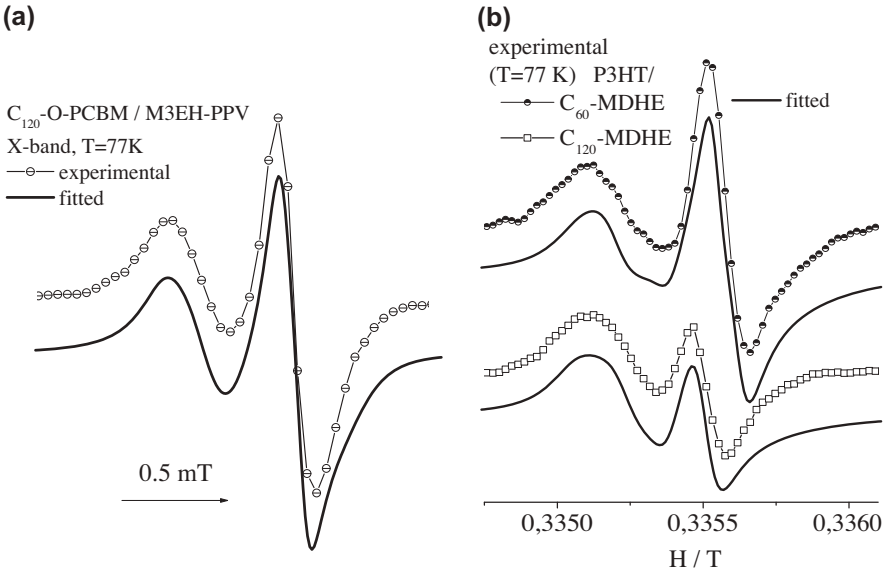

Fig. 5 – Experimental and fitted X-band spectra of (a) C_{120}-O-PCBM/M3EH-PPV, (b) C_{60}-MDHE/P3HT and C_{120}-O-MDHE/P3HT (spectra denominations are inside the figures).

rected. While the reason of the above deviation of dispersion contribution has not been definitely established so far, we connect this result with the blend morphology, form and average size of domains/nanoparticles formed during the film preparation. In addition, our preliminary results with C_{120}-O di-fullerenes blended with M3EH-PPV show the same L tendency and one sample exhibited $L > 3$ (experimental and simulated spectra of C_{120}-O/M3EH-PPV are shown in Fig. 7). The limit of reliable registration of the L value in W-band experiment is at a level of about $L = 0.05$ ($X = 0.4$), which predicts a conductivity registration at least 20 times less than estimated for di-fullerenes. However taking into account the absence of dispersion contribution in W-band spectra for blends including mono-fullerenes we suppose a significantly lower photoconductivity at least of mono-fullerene medium. This supposition could be expected taking into account pure C_{60} thin films with a photoconductivity value of about $10^{-3} - 10^{-4}$ S $(cm)^{-1}$, without oxygen treatment, as reported in [16].

Here it should be pointed out that one can consider the above estimation of difullerene/nanoparticle conductivity (or L) as the lower boundary of L. As it was established for 2D electron gas systems [11], the absorption contribution to

Table 1 – ESR parameters of M3EH-PPV/fullerenes spectra.

	g_x	g_y	g_z	Δ_x	Δ_y	Δ_z	L
[a] M3EH-PPV (P^+)							
W-band, T = 50 K	2.00377	2.00275	2.0022	0.4	0.4	0.4	0
[b] **C_{60}-PCBM**							
W-band, T = 50 K	2.00021	2.0000	1.9986	0.5	0.4	1.7	0
[a] **C_{120}-O-PCBM**							
W-band, T = 50 K	2.00045	2.00004	1.9986	0.57	0.58	1.6	1.0
X-band, T = 77 K	2.00063	2.0000	1.9987	0.07	0.07	0.24	0.3
C_{60}-MDHE							
W-band, T = 80 K	2.00016	2.0000	1.9994	0.21	0.19	1.0	0
T = 20 K	2.00018	2.0001	1.9995				0
X-band, T = 77 K	2.00028	1.9999	1.9996	0.045	0.06	0.38	0
C_{120}-O-MDHE							
W-band, T = 80 K	2.0005	2.00023	1.9991	0.21	2.3	0.9	0.35
T = 20 K	2.0006	2.00024	1.9991	0.2	2.2	0.9	0.33
X-band, T = 77 K	2.00058	2.00028	1.9990	0.06	0.07	0.43	0.035

[a] $\Delta_{x,y,z}$ have deviations in different spectra.
[b] Here g-factor values differ slightly up to $\sim 3 \times 10^{-4}$ from some g_i components obtained in [5] using X- and K-bands techniques due to: (a) higher W-band spectral resolution, (b) an accounting of dispersion contribution in anion radical spectra that cannot be predicted in [5]. However, with respect to the C_{120}-O-PCBM anion radical, Δ_i values obtained in X-band exhibit the appreciable difference in comparison with the analogous in [5] ($\Delta_{x,y,z}$ = 0.25, 0.24, 0.32 mT). We observed the same effect in some other fullerene derivatives and attribute the difference to the time interval between the synthesis and the ESR experiment, i.e. several weeks in [5] and about 1 year in this work, but this consideration needs an additional study.

the ESR line in 2D crystalline systems, orientated relative to the direction of the external magnetic field (H), has angular dependence on H. Therefore, for the correct spectra simulation, the parameter L in expression (3) must be replaced with $L_oF(\alpha)$,

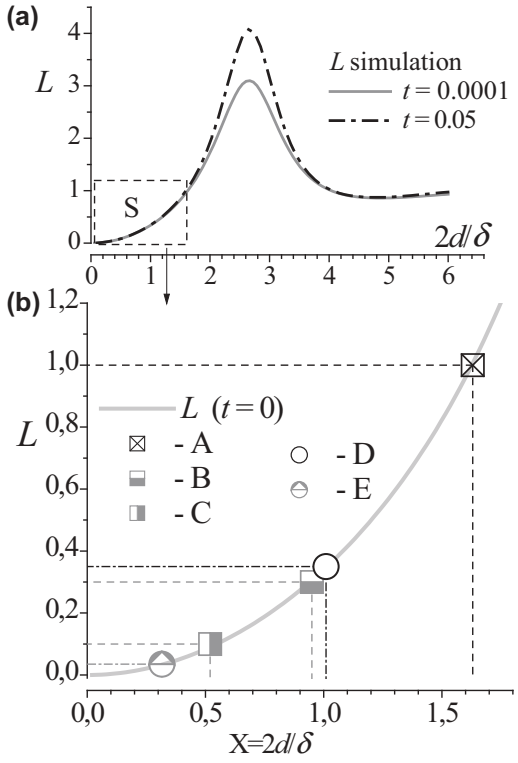

Fig. 6 – (a) L = P/Q as a function of X = 2d/δ, constructed with two different t values (appropriate denominations are in the text), (b) S-area of (6a), includes only experimental L and X values (an appropriate explanation of A, B, C, D, E experimental points is in the text).

where $L_o = L_{max}$, however the above was omitted in our consideration due to the analytical function of $L = L_oF(\alpha)$ being unknown. Taking into account that some additional absorption contribution can take place, due to the possibility of some difullerene domains/nanoparticle geometrical size is more than film thickness, and therefore can be partly orientated relative to the H direction. This only increases the dispersion part in the simulated spectra i.e. one can only estimate the lower boundary of L correctly. Therefore, the 2D version cannot be excluded, but needs the homogeneously orientated crystalline structure, at least partly orientated in the film, for confirmation.

The formation of difullerene domains/nanoparticles is also verified by the scanning electron microscope image

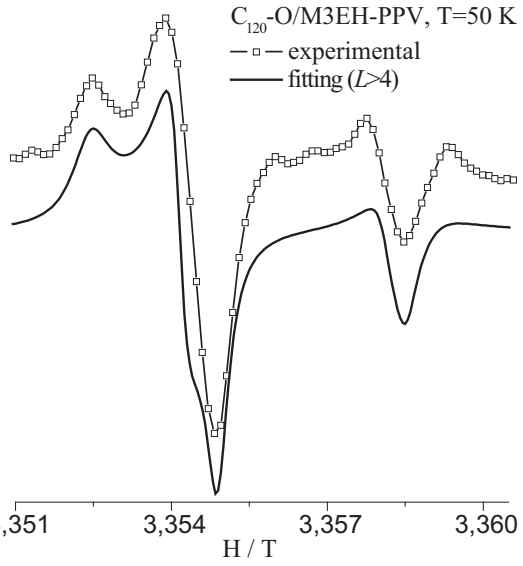

Fig. 7 – Experimental and fitted W-band sspectra of C_{120}-O/M3EH-PPV (C_{120}-O radical: $L > 4$; g_x = 2.00037, g_y = 2.00015, g_z = 1.9999).

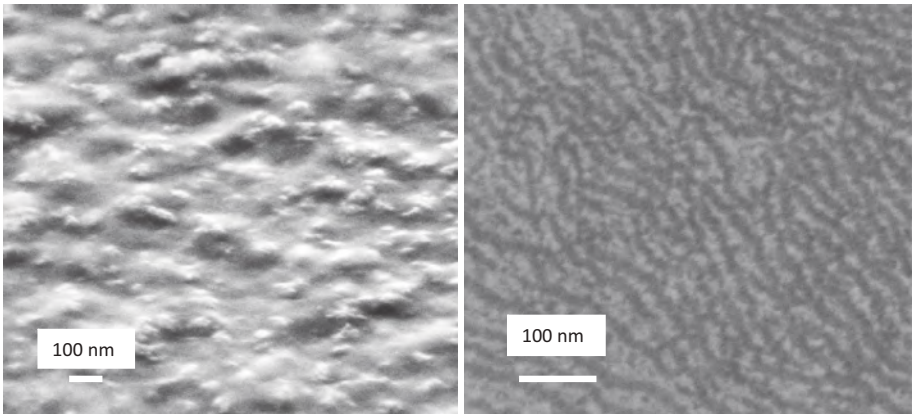

Fig. 8 – Scanning electron microscope image of: (a) P3HT:C_{120}-O (1:1) and (b) P3HT:PCBM 100 nm thickness films.

(SEMI) of the ~100 nm thick film introduced in Fig. 8a. For comparison the SEMI of the P3HT:PCBM film surface is shown in Fig. 8b and indicates a more homogeneous film structure relative to the film comprising difullerene (the domains are absent). Auger spectroscopy results indicate ~15% more oxygen, responsible for the difullerenes, at the high points of the surface relief film (top of the "mountains") than at the low points (bottom of the "mountains"). Contrary to the last, the sulfur, responsible for the polymer Auger spectra, exhibits the opposite result, as there is ~20% higher sulfur concentration at the bottom of the surface relief film in comparison with the top. Moreover the introduced results with difullerene derivatives could partly explain the relatively insignificant SC power conversion efficiency of the P3HT:C_{120}-O-PCBM device (~0.57%) reported once in [17], due to the possibility of photocurrent shunting by the high conductive difullerene domain partly contacted with both electrodes.

4. Conclusion

In summary we point out that the registration of dispersion contribution to LESR absorption spectrum of polymer/di-fullerenes donor–acceptor blends can be attributed to the higher photoconductivity of difullerenes in comparison with mono-fullerenes. In light of recent synthesis and study of highly conductive 2D organic metals based on mono-fullerenes [6], the possibility of analogous planar structure formation in the di-fullerene domains/nanoparticles cannot be excluded.

Acknowledgment

Financial support from the BMBF international department is gratefully acknowledged (Project ID: Rus 09/051).

REFERENCES

[1] Scharber MC, Sariciftci NS. Efficiency of bulk-heterojunction organic solar cells. Prog. Polym. Sci. 2013;38:1929–40.
[2] Reed CA, Bolskar RD. Discrete fulleride anions and fullerenium cations. Chem. Rev. 2000;100:1075–120.
[3] Balch AL, Costa DA, Fawcett WR, Winkler K. Electronic communication in fullerene dimers. Electrochemical and electron paramagnetic resonance study of the reduction of C_{120}O. J. Phys. Chem. 1996;100:4823–7.
[4] Dunsch L, Rapta P, Gromov A, Stasko A. In situ ESR/UV–vis–NIR spectroelectrochemistry of C_{60} and its dimers C_{120}, C_{120}O and C_{120}OS. J. Electroanal. Chem. 2003;547:35–43.
[5] Konkin A, Ritter U, Scharff P, Roth H-K, Aganov A, Sariciftci NS, et al. Photo-induced charge separation process in (PCBM-C_{120}O)/(M3EH-PPV) blend solid film studied by means of X and K-bands ESR at 77 and 120 K. Synth. Met. 2010;160:485–9.
[6] Konarev DV, Khasanov SS, Otsuka A, Maesato M, Saito G, Lyubovskaya RN. A two-dimensional organic metal based on fullerene. Angew. Chem. Int. Ed. 2010;49:4829–32.
[7] Weber L, Reinmoller M, Ritter U. Diazoalkane addition reaction on the fullerene dimer C_{120}O and characterization of the resulting mono-adduct. Carbon Sci. Technol. 2008;1:9–12.
[8] Kietzke T, Egbe DAM, Hörhold H-H, Neher D. Comparative study of M3EH-PPV-based bilayer photovoltaic devices. Macromolecules 2006;39:4018–22.
[9] Egbe DAM, Kietzke T, Carbonnier B, Mühlbacher D, Hörhold H-H, Neher D, Pakula T. Synthesis, characterization, and photophysical, electrochemical, electroluminescent, and photovoltaic properties of yne-containing CN–PPVs. Macromolecules 2004;37:8863–73.
[10] Wilamowski Z, Jantsch W. Spin resonance properties of the two-dimensional electron gas. Physica E 2001;10:17–21.
[11] Wilamowski Z, Jantsch W. Suppression of spin relaxation of conduction electrons by cyclotron motion. Phys. Rev. B 2004;035328:1–10.
[12] Kempifiski W, Scharff P, Stankowski J, Piekara-Sady L, Trybula Z. EPR of fullerene ions and superconductivity in K-fullerides at low doping levels. Physica E 1997;274:232–6.
[13] Altshuler TS, Vinogradova OB, Kukovitskii AF, Kharakhashjan EG. Analysis of magnetic resonance spectrum of localized spins. Sov. Phys. Solid State 1974;15:2402–16.
[14] Chapman AC, Rhodes P, Seymour EFW. The effect of eddy currents on nuclear magnetic resonance in metals. Proc. Phys. Soc. B 1957;70:345–60.
[15] Hesper R, Tjeng LH, Heeres A, Sawatzky GA. BCS-like density of states in superconducting A_3C_{60} surfaces. Phys. Rev. Lett. 2000;85:1970–3.
[16] Bhuiyan MKH, Mieno T. Effect of oxygen on electric conductivities of C_{60} and higher fullerene thin films. Thin Solid Films 2003;441:187–91.
[17] Weber L, Sensfuss S, Ritter U, Scharff P. Preparation, characterization, functionalization and application of dimeric fullerene oxides. Full. Nanot. Carb. Nanostr. 2009;17:187–207.